Direct Measurement of the Fast, Reversible Addition of Oxygen to Cyclohexadienyl Radicals in Nonpolar Solvents

James W. Taylor,[†] Gerhard Ehlker,[‡] Hans-Heinrich Carstensen,[§] Leah Ruslen,[||] Robert W. Field,[⊥] and William H. Green*[,†]

Massachusetts Institute of Technology, Cambridge, Massachusetts 02139 and Colorado School of Mines, Golden, Colorado 80401

Received: December 20, 2003; In Final Form: June 16, 2004

The title reaction was measured directly by laser flash photolysis in several nonpolar solvents, using both the strong ultraviolet and weaker visible absorption bands of the cyclohexadienyl radical. Both the visible and ultraviolet transient absorptions are shown to have identical time dependence, confirming that both absorptions correspond to the same species. The cyclohexadienyl radical's spectra were observed in several nonpolar solvents and are reported. The rate constant of the title reaction is $1.2 \pm 0.4 \times 10^9$ M^{-1} s^{-1} in cyclohexane solvent at room temperature (298 K). This reaction is diffusion-limited, which is consistent with previous literature reports, but 2 orders of magnitude faster than the rate constant measured recently in the gas phase. Reasons for the discrepancy are explored, with the most likely explanation being that the title reaction becomes equilibrated in both the liquid and gas phases. Calculations reveal that the weak solvation of the nonpolar solvents coupled with higher oxygen concentrations in solution are sufficient to make the equilibrium of cyclohexadienyl with its peroxyl products observable. In cyclohexane solvent, a multiexponential decay is observed at these conditions. The current data place upper and lower bounds on the equilibrium constant for the title reaction in cyclohexane. Possible mechanisms are discussed for explaining the slower decay of equilibrated cyclohexadienyl radicals found in both liquid and vapor phases.

1. Introduction

The present study focuses on the reaction of resonantly stabilized cyclohexadienyl radicals with molecular oxygen to form the isomeric cyclohexadienylperoxyl radicals

$$C_6H_7^\bullet + O_2 \rightarrow o\text{-}C_6H_7OO^\bullet \quad (1a)$$

$$C_6H_7^\bullet + O_2 \rightarrow p\text{-}C_6H_7OO^\bullet \quad (1b)$$

where ortho means the CH_2 group is adjacent to the CHOO group and para means they are on opposite sides of the six-membered ring, as shown in Figure 1. The ortho isomer contains a chiral carbon and exists as two enantiomers.

The reactions of hydrocarbon radicals with molecular oxygen are a subject of intense interest, since they are technologically important. The rate of oxidation in many materials, such as foods, pharmaceuticals, and polymers, determines their useful life. However, since oxygen is also the cheapest oxidant, many commercial processes rely on hydrocarbon oxidation. Consequently, a large industry is devoted to both inhibiting and enhancing these reactions.

In addition to the commercial relevance, the details of hydrocarbon radical oxidation kinetics are critical in academic fields ranging from biology to atmospheric chemistry. Specifically, in combustion processes, the reversibility of oxygen addition is thought to be responsible for the negative temperature coefficient (NTC) region, where oxidation rates are not a monotonic function of temperature.

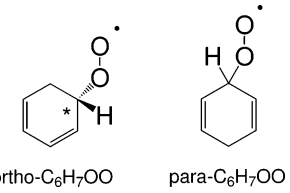

Figure 1. Structures of the cyclohexadienylperoxyl radicals. Note: the ortho isomer contains a chiral center (labeled with an asterisk) and exists as two enantiomers. In the preferred conformation, the O−O−C−H dihedral angle is 180°.

Although many hydrocarbon radical oxidation reactions, including the title reaction, have been studied for decades, there are still many mysteries to be solved. For example, the decomposition pathway with the smallest barrier for the reaction of ethyl radical with oxygen was not conclusively identified until recently,[1] and systems as apparently simple as butyl + O_2 are still challenging areas of research.[2]

Under cool flame conditions, radical oxidation (R + O_2) reactions are now thought to rapidly form alkenes and other unsaturated species. As these unsaturated species accumulate, the combustion reactions become dominated by the reactions of resonantly stabilized radicals with oxygen. Due to their late appearance in most combustion processes, these radicals are difficult to study using flame techniques. Thus, despite their importance in the latter stages of ignition, relatively little is known about the reactions of resonantly stabilized radicals with oxygen.

* To whom correspondence should be addressed. Tel: 617.253.4580.
[†] MIT Department of Chemical Engineering.
[‡] Present Address: Leipziger Str. 2, 46397 Bocholt, Germany.
[§] Colorado School of Mines Department of Chemical Engineering.
[||] Present Address: 18115 Pine Trail, Los Gatos, CA 95033.
[⊥] MIT Department of Chemistry.

10.1021/jp0379547 CCC: $27.50
Published on Web 08/26/2004

Recently published experimental investigations of the reaction of cyclohexadienyl with O_2 by Berho et al.[3] and Estupiñán et al.[4] indicate that cyclohexadienyl radicals react slowly with molecular oxygen in the gas phase ($k_1 = k_{1a} + k_{1b} = 2.4 \times 10^7$ M^{-1} s^{-1}). However, earlier measurements of this reaction in water[5] and in a peroxide/benzene solution[6] came to different conclusions: the measured rates are fast and appear to be diffusion limited ($k_1 \sim 10^9$ M^{-1} s^{-1}). The reaction rate in solution appears to be 50 times faster than that in the gas phase. There are similar differences in the literature regarding the analogous reaction

$$HOC_6H_6^{\bullet} + O_2 \rightleftharpoons o\text{-}HOC_6H_6OO^{\bullet} \quad (2a)$$

$$HOC_6H_6^{\bullet} + O_2 \rightleftharpoons p\text{-}HOC_6H_6OO^{\bullet} \quad (2b)$$

which has been extensively studied in both the gas phase[7−10,21,46] and in aqueous solution.[5,11,12,45]

Several published reports[13,14,46] suggest that reactions 1 and 2 and similar reactions of other resonantly stabilized radicals[15] have significant activation barriers in the gas phase, which might explain the slow rate reported by Estupiñán et al. However, all solution phase measurements indicate that these reactions are diffusion-limited,[5,6] suggesting that no significant barriers exist. The reason for the large differences between the recent gas-phase measurements and the liquid-phase results is unknown.

In addition to the kinetics, the thermochemistry of reaction 1 is uncertain: theoretical calculations predict that this and similar reactions are only slightly exothermic,[13,14,16] while the only direct experimental measurements find $\Delta H^\circ = -12$ kcal/mol for reaction 1 in organic solvents.[16] In aqueous solution, reaction 2 is known to be reversible, and rapidly equilibrates at room temperature.[12] The measured equilibrium constant corresponds to $\Delta G^\circ = -23.8$ kJ/mol for reaction 2 in aqueous solution (1M standard state). Curiously, under similar conditions, reaction 1 did not have a detectable equilibrium in aqueous solution.[5]

Hendry and Schuetzle found that in chlorobenzene, 1,4-cyclohexadiene and oxygen were quantitatively converted to benzene and H_2O_2. Based on these finding, the authors suggested that the dominant reaction is the direct abstraction of hydrogen.[17]

$$C_6H_7^{\bullet} + O_2 \rightarrow HO_2^{\bullet} + C_6H_6 \quad (3)$$

Although Hendry and Schuetzle gave arguments against it, their data do not conclusively rule out a sequential reaction, with reaction 1 followed rapidly by

$$o\text{-}C_6H_7OO^{\bullet} \rightarrow HO_2^{\bullet} + C_6H_6 \quad (4a)$$

$$p\text{-}C_6H_7OO^{\bullet} \rightarrow HO_2^{\bullet} + C_6H_6 \quad (4b)$$

Recently, Estupiñán et al. have also argued that reaction 3 is the dominant reaction channel.[4] Note that both reactions 3 and 4 are highly exothermic because of the stability of the product, benzene. Concerted HO_2 elimination from adjacent carbons as in reaction 4a is known to be one of the primary channels for the decay of ethylperoxyl and other simple alkylperoxyls with β hydrogens in the gas phase at temperatures greater than 400 K.[1,18,19] Reaction 4b, where the oxygen removes a hydrogen from across the ring, is expected to have a considerably higher barrier than reaction 4a, though little is known regarding this reaction.[5,20]

Pan et al. found evidence that in an aqueous alkaline solution about 60% of the C_6H_7OO formed decomposes on a microsecond time scale to form HO_2 and benzene. They interpreted the 60% yield as meaning that the ortho isomer of C_6H_7OO decomposes rapidly by reaction 4a ($k_4 > 8 \times 10^5$ s^{-1}), but that the para isomer decays by another pathway, i.e., reaction 4b is slow. It is unclear from their product data exactly what happened to the remaining 40% of the C_6H_7OO. Note that the data of Pan et al. does not conclusively rule out reaction 3, but the difference between the rate of C_6H_7 disappearance and the rate of HO_2 appearance indicates that $k_1 > k_3$. Also, the high value for k_4 reported by Pan et al. is surprisingly 2 orders of magnitude faster than the rates for the analogous reactions of several hydroxylated cyclohexadienylperoxyls[12] measured by the same group using the same technique; to date no one has explained why reaction 4 should be so much faster in unsubstituted cyclohexadienylperoxyls. The photoacoustic calorimetry of Kranenburg et al.[16] conclusively shows that in organic solvents at room temperature, reaction 1 is faster than 3, and also sets an upper bound of about 2×10^9 s^{-1} on reactions 4.

Cyclohexadienylperoxyl radicals have many other potential decay pathways in addition to reaction 4a; several of these have been studied theoretically by Lay et al.[20] and by Raoult et al.[21] The most obvious decay channel is to lose O_2 by the reverse of reaction 1. The reverse of reaction 2 is known to occur on a 100 μs time scale in aqueous solution; however, the corresponding reverse of reaction 1 has not been detected. The fact that a significant amount of heat was evolved in the photoacoustic calorimetry experiments of Kranenburg indicates that $k_{-1} < 2 \times 10^9$ s^{-1} in organic solvents. Pan et al. proposed that para-cyclohexadienylperoxyl decays primarily via intramolecular addition of oxygen to one of the double bonds. However, both ab initio[20] and empirical[22] calculations indicate that, in contrast to the ortho isomer, this process is significantly endothermic for the para isomer. Lay et al. also predicted that this process would have a high barrier, at least for hydroxylated cyclohexadienylperoxyls.

Most of the previous work on reaction 1 was done in the gas phase or in aqueous solution, so one might wonder if the 50-fold rate discrepancy is due to solvent effects or chemical activation effects. In this work, we measure k_1 in nonpolar solvents, which reduces the solvent effect compared with water and avoids chemical activation effects associated with the gas phase. Working in solution also allows us to make measurements on a faster time scale than in the gas-phase experiments, and with higher signal-to-noise, such that we can establish limits on the equilibrium constant for reaction 1, and for the rates of some of the secondary processes. Finally, we measure the time-dependence of both the absorption band in the visible region and the ultraviolet band (used for all other kinetic measurements reported in the literature) under identical conditions to confirm that both transient absorptions arise from the same species. In addition, we performed ab initio calculations on the bond dissociation energy of cyclohexadienylperoxyl in the gas phase and in solution to better understand the reaction.

This paper is organized as follows: The experimental apparatus and the calculation method used are presented in sections 2 and 3. In section 4, we present experimentally observed spectra and kinetic profiles of cyclohexadienyl radicals reacting with oxygen. In sections 4.4 and 4.5 we discuss models and mechanisms that could explain the observations. Subsequently, in section 5, we present the results of our electronic structure calculations. The paper concludes with a discussion of our understanding of the title reaction based on the available data and calculations.

2. Experimental Method

Reaction rates of cyclohexadienyl radicals with oxygen in different solvents were measured by laser flash photolysis. An excimer laser pulse photolyzed di-*tert*-butyl peroxide to produce *tert*-butoxyl radicals (reaction 5). These radicals reacted rapidly with excess amounts of 1,4-cyclohexadiene to rapidly generate cyclohexadienyl radicals (reaction 6). The transient absorptions of the cyclohexadienyl radicals were recorded using light from a pulsed Xe flash lamp, passing through a monochromator to a photomultiplier

$$(CH_3)_3COOC(CH_3)_3 + h\nu_{248} \rightarrow 2(CH_3)_3CO^{\bullet} \qquad (5)$$

$$(CH_3)_3CO^{\bullet} + C_6H_8 \rightarrow (CH_3)_3COH + C_6H_7^{\bullet} \qquad (6)$$

The solutions prepared typically contained between 0.1 and 1 M 1,4-cyclohexadiene (Aldrich, 97%) and 0.1 M DTBP (di-*tert*-butyl peroxide, Aldrich, 98%) in one of four solvents: cyclohexane (Baker, HPLC Grade), dichloromethane (EM Science, 99.9%), perfluorohexane (Aldrich, 99%), and 1,1,2-trichlorotrifluoroethane (Aldrich, 99%). The chemicals were used as received. Oxygen was added to the liquid system by bubbling an O_2/Ar mixture prepared using Sierra mass-flow controllers (accurate to ±0.1%). A splitter was used to divert ~20% of the 500 mL/min flow to the liquid sample. The partial pressures of the gases used in the experiment were corrected to take into account the vapor pressure of the solvent at the experimental temperature and atmospheric pressure. The O_2 solubilities were taken from literature.[23,24] The reagent solution was then circulated through a 1 cm × 4 mm flow cuvette (Spectrocell Corp.) at a constant flow rate of 15 mL/min to avoid accumulation of photolysis and reaction products.

A Lambda Physik Compex 102 Excimer Laser containing a KrF gas mixture generated 25 ns photolysis pulses at a wavelength of 248 nm. About 30 mJ of this light was directed onto the cuvette through an iris. The amount of photolysis light entering and leaving the sample cuvette was measured using a calibrated power meter from Ophir Optronics. The photolysis fluence was approximately 1 MW/cm^2.

Transient spectra were recorded using a Flash Kinetic Spectrometer (Applied Photophysics LKS.50). The probe beam was generated by a Xenon short arc flash lamp (OSRAM, XBO 150 W/CR OFR) mounted in a convection cooled housing. The duration of the pulsed probe light was about 1.5 ms, and the intensity of the central portion of the pulse was flat within 0.5% for 100 μs. Since the 100 μs plateau is much longer than the reaction times measured, the lamp output is essentially constant during each recorded transient absorption period.

The probe beam is focused through the sample cuvette using a standard crossed beam arrangement. The probe beam is approximately 1 mm in diameter and is set to pass close to the face of the cuvette exposed to the laser pulse, where the highest concentration of the transient species is formed.

After exiting the cuvette the probe beam passes through a Schott WG 305 filter to suppress scattered light from the photolysis beam. The beam is then focused onto the entrance slit of an f/3.4 holographic diffraction grating monochromator, having a symmetrical Czerny-Turner configuration. The light passing through the monochromator is detected by a Hammamatsu 1P28 side window photomultiplier (200−650 nm wavelength range). The signal output from the photomultiplier is digitized by a Hewlett-Packard HP54510 Digitizing Oscilloscope. The collected data are stored and analyzed on the spectrometer workstation. The monochromator wavelength is adjusted with a stepper motor drive controlled by a microprocessor, which is interfaced to the spectrometer workstation. The spectra are typically recorded by averaging 30−100 transient absorption traces containing 500 temporal data points for each transient absorption. The data are collected so that 10% of the acquisition period provides pre-trigger information.

Each spectrum was normalized to the probe light intensity immediately before the photolysis pulse, thus reducing signal artifacts due to electronic pickup of the excimer discharge or to pulse-to-pulse variations in the flash-lamp intensity. The signal is further corrected by subtracting the baseline measured by blocking the photolysis beam with a shutter. The transient absorption data from the spectrometer was then analyzed using standard numerical techniques such as singular value decomposition and multivariate least-squares regression, using data analysis tools and differential equation solvers included in the Pro-Kineticist[25] analysis tools from Applied Photophysics and MATLAB computer packages.

3. Calculation Method

The B3LYP density functional method, as implemented in the Gaussian 98W suite of programs[26] on a PC, is used to calculate the energies, equilibrium geometries, and vibrational frequencies of C_6H_7 and C_6H_7OO. Gas-phase properties are calculated at B3LYP/6-311+G(2d,p)//B3LYP/6-31G(d), B3LYP/6-311+G(3df,2p)//B3LYP/6-31G(d), and B3LYP/6-311+G(3df,2df,2p)//B3LYP/6-31G(d) levels using the ultra-fine grid option in the last two geometry optimizations. To capture electrostatic solvation effects, we also perform calculations for cyclohexane and dichloromethane solutions using the polarizable continuum model of Wiberg and co-workers[27] at the B3LYP/6-311+G(2d,p)//B3LYP/6-31G(d) level. In the polarizable continuum models, we use a dielectric constant of 2.023 for cyclohexane and 8.93 for dichloromethane.

Most density functional methods, including B3LYP, do not give accurate absolute values for peroxyl radical thermochemistry.[28] To improve the accuracy of the calculations, the results are calibrated by comparison to B3LYP calculations for allyl and allylperoxyl radicals, where the experimental gas phase thermochemistry is available.[29,30] This procedure is similar to the common practice of using isodesmic reactions to predict thermochemistry.

The results from quantum chemistry calculations are also checked against empirical estimates. The gas-phase values are compared with group-additivity estimates made using the THERM program.[31] Empirical solvation corrections are based on analogies with known compounds as discussed below.

The pressure-dependent falloff of reaction 1 is computed using the Master Equation method as implemented in MULTIWELL.[32,33] The densities of states are computed using the Stein − Rabinovitch variant of the Beyer−Swinehart direct-count algorithm.[34] The C−O single bond is treated as a free internal rotor. For the falloff calculation, the rate for the barrierless adduct formation reaction

$$C_6H_7^{\bullet} + O_2 \rightarrow C_6H_7OO^{\ddagger} \qquad (7)$$

in the gas phase was assumed to be 1.5×10^9 M^{-1} s^{-1} and temperature/energy independent. This calculation confirms that reaction 1 is in the high-pressure limit under the conditions of Berho and Lesclaux, as stated by those authors.[3]

4. Experimental Results

4.1. C_6H_7 Absorption Bands in Various Solvents. The transient absorption of C_6H_7 was measured in several nonpolar

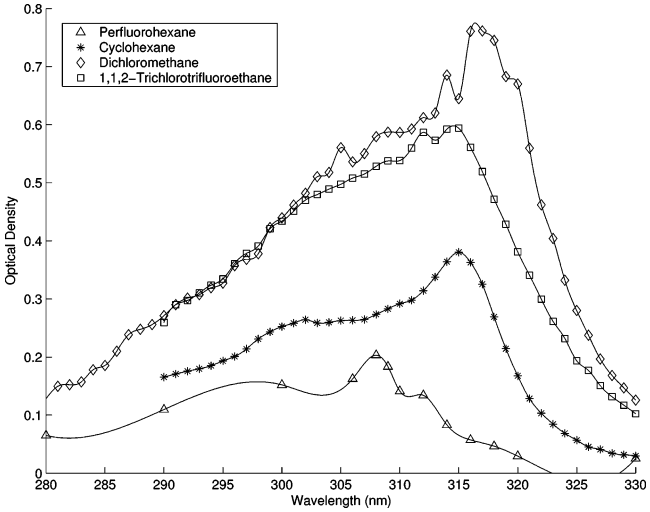

Figure 2. UV absorption spectra of cyclohexadienyl radical in various solvents at room temperature (298 K) and pressure (1 atm). C_6H_8 and DTBP concentration for each solvent was 0.1 M. The relative heights of the spectral peaks probably correspond to slightly different concentrations of cyclohexadienyl in solution, as opposed to a solvent effect changing the absorption coefficient.

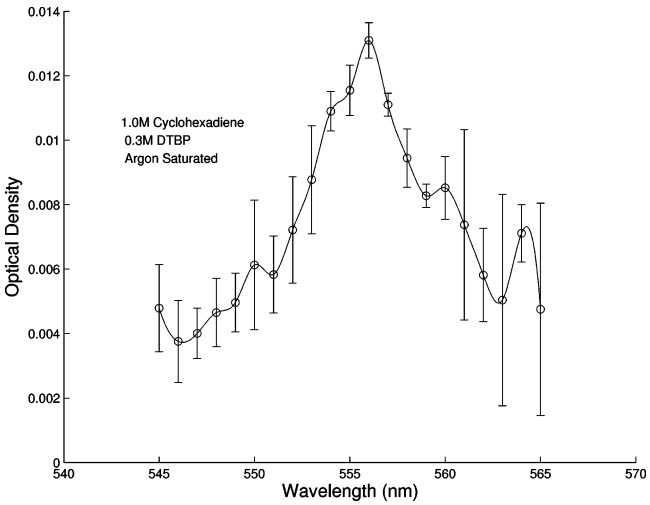

Figure 3. Visible absorption spectrum of cyclohexadienyl radical in cyclohexane solvent at room temperature (298 K).

TABLE 1: Observed Positions of the Maxima of the Cyclohexadienyl Radical Spectrum in Various Organic Solvents

solvent	UV band position [nm]	visible band position [nm]
cyclohexane	316	556
dichloromethane	317	558
1,1,2-trichlorotrifluoroethane	314	555
perfluorohexane	308	N/A

solvents: cyclohexane, dichloromethane, perfluorohexane, and 1,1,2-trichlorotrifluoroethane. The observed band positions in these solvents are listed in Table 1 and the UV spectra are shown in Figure 2.

In all cases, the UV band displays a characteristic two-hump structure. In some experiments, this band is overlapped by a weaker broad band with a peak around 280 nm, which has a different time-dependence from those in Table 1.

Figure 3 shows a visible spectrum for the cyclohexadienyl radical in cyclohexane. Absorption at the visible wavelength is much weaker than in the UV band. Error bars are shown in Figure 3 to indicate the signal-to-noise of this weak absorption.

The absolute absorption coefficient of C_6H_7 in cyclohexane at 316 nm was estimated by measuring the excimer laser fluence and the corresponding transient absorption of the probe beam, using the known di-*tert*-butyl peroxide absorption strength and quantum yield[35] and the known rate constant for the competing reaction of *tert*-butoxyl with cyclohexane.[6] Our inferred absorption strength is consistent with the value of $\epsilon_{316} = 5400\ M^{-1}\ cm^{-1}$ measured by Sauer et al.[36] It is also similar to the value of $\epsilon_{316} = 4400\ M^{-1}\ cm^{-1}$ reported in aqueous phase by Pan and von Sonntag.[11] The gas phase peak lies at 302 nm and the absorption strength at the peak has variously been reported as $15\,000\ M^{-1}\ cm^{-1}$ by Berho[3] and $2700\ M^{-1}\ cm^{-1}$ by Bjergbakke.[7]

The absorption strength at 556 nm was estimated relative to the 316 nm absorption by rapidly scanning the monochromator between the two wavelengths. Because neither the Xe flash-lamp intensity nor the photomultiplier response is constant over this broad wavelength range, it was necessary to simultaneously adjust the voltage and thus the gain of the photomultiplier tube. The 316 nm absorptions were consistently approximately 50 times stronger than the 556 nm absorptions under identical circumstances, yielding an estimated C_6H_7 absorption strength $\epsilon_{556} = 100\ M^{-1}\ cm^{-1}$ ($\sigma = 2 \times 10^{-19}\ cm^2$) in cyclohexane. To our knowledge, the green band of the cyclohexadienyl radical has not yet been detected in the gas phase.

4.2. Interferences. We collected data at a wide range of detection wavelengths, to identify potential interferences. The measured transient absorptions, $A(t,\lambda)$, were analyzed using singular-value decomposition (SVD). The SVD analysis revealed that a single transient species was responsible for more than 90% of the observed signal, but weak interferences corresponding to the other singular values were detected. The most significant interference is the weak absorption of the peroxyl radicals (ROO) from cyclohexadienyl via reaction 1 and from side reactions (e.g., abstraction of an H atom from the solvent). The absorption strength of the ROO radicals at 316 nm is not accurately known (this is the weak long-wavelength tail of the well-known peroxyl radical UV band); here we use $\epsilon = 200\ M^{-1}\ cm^{-1}$.[37] The *tert*-butoxy radical also absorbs at 316 nm, $\epsilon_{316} \sim 500\ M^{-1}\ cm^{-1}$,[38] but the *tert*-butoxy transient has a short lifetime, so this interference is not important.

For safety reasons, a small amount of hydroquinone is added as a stabilizer to the 1,4-cyclohexadiene by the manufacturer, so the semiquinone radical should be formed in our experiments. However, hydroquinone is only sparingly soluble in our nonpolar solutions and, in fact, was undetectable by UV−vis spectrophotometry at the part per million level. Due to the extremely low concentration of hydroquinone, the semiquinone interference is not expected to be detectable at our signal-to-noise level.

The peroxyl radicals cause the main interference with the cyclohexadienyl measurements at 316 nm, so it is important to understand the time-dependence of their signals. This was done in two ways: (a) by tuning off the cyclohexadienyl peak to shorter wavelengths, where the peroxyl radicals absorb more strongly, and (b) by experiments performed at 316 nm in the absence of 1,4-cyclohexadiene. The peroxyl radical interference can also be avoided by using the green band; however, the signal-to-noise ratio on this weak band is not sufficient to draw definite conclusions about cyclohexadienyl kinetics. In the absence of cyclohexadiene, the butoxyl radical attacks the cyclohexane solvent, forming cyclohexyl radicals. The resulting transient absorption is attributed to the cyclohexyl peroxyl

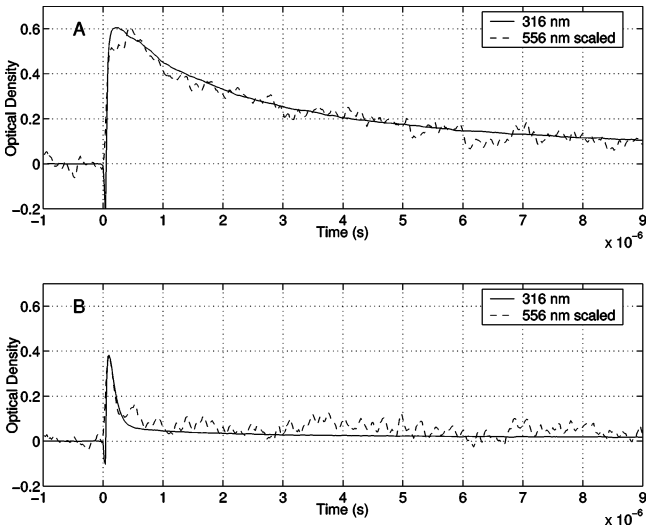

Figure 4. Transient absorptions measured using the ultraviolet and visible bands of the cyclohexadienyl radical in cyclohexane solution (0.4 M 1,4-CHD and 0.1 M DTBP, $T = 298$ K). Argon saturated solutions are shown in (A), whereas oxygen saturated solutions are shown in (B). The peak heights of the two absorption bands were normalized and show identical time-dependence confirming that both absorption bands arise from the same species.

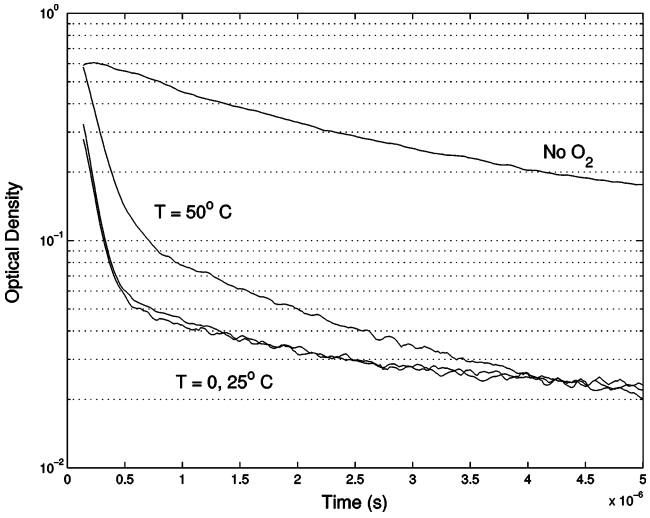

Figure 5. Comparison of the decay of cyclohexadienyl at different temperatures. Initial concentrations were 0.1 M 1,4-CHD and 0.1 M DTBP in cyclohexane solvent saturated with either Ar or O_2. At 323 K, the slow component decays at twice the rate at lower temperatures. The fast component of the decay in the presence of O_2 is relatively temperature independent.

radical formed by O_2 addition; like most peroxyl radicals, it has a slow second-order decay constant, so it is stable on the 10μs time scale of our experiments. From these studies, we infer that the peroxyl interference is the source of $\approx$1% of the absorption observed in our experiments and has a negligible effect on the conclusions.

4.3. Time-Dependence of the Transient Absorptions. Most previous work on C_6H_7 had utilized either the UV band or the green band, but not both. The only exceptions were matrix studies. In the matrix studies, electron spin resonance (ESR) confirmed that C_6H_7 was present, but the experiments were not able to demonstrate that both absorption bands arose from the same species.[39] Here, we measure the time-dependence of the transient absorptions using both bands. In Figure 4, we demonstrate that the two absorptions have equivalent time-dependence under widely different conditions of oxygen concentration, implying that the absorptions arise from the same species. The two absorption bands could arise from two species in rapid equilibrium, e.g., two isomers of C_6H_7, but these species would have to equilibrate on a sub-microsecond time-scale at room temperature to be consistent with the observations.

A typical time-resolved absorption measurement of the C_6H_7 radical is shown in Figure 4. Initially, 10% of the data set is recorded before the photolysis pulse to ensure an accurate measurement of the signal before absorption. After the photolysis pulse, scattered fluorescence creates a small negative signal, which then rises to peak absorbance over a period of approximately 100 ns. The peak occurs where the rate of generation of C_6H_7 is equal to its rate of decay. From the peak, the absorption decays at a rate an order of magnitude slower than the initial rise.

In the absence of oxygen, the C_6H_7 radical decays on a 10 μs time scale, presumably through radical−radical recombination. However, in the presence of oxygen, the C_6H_7 radical decays on a 1 μs time scale, due to the title reaction. Changes in temperature do not significantly change the fast decay rate under oxygenated conditions, as shown in Figure 5.

4.4. Pseudo-First-Order Rate Constants for $C_6H_7 + O_2$. The conventional method for determining rate constants from

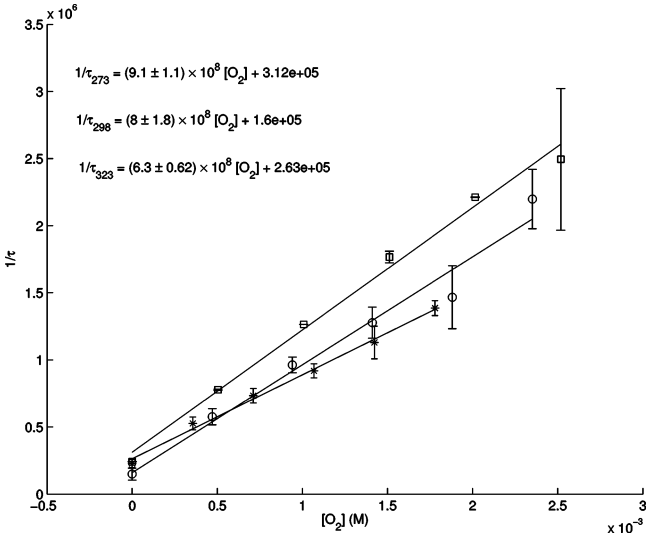

Figure 6. Time-dependent cyclohexadienyl absorption data were fit to single-exponential curves to determine the effective rate of decay of the radical at various oxygen concentrations (0−1 mM) and temperatures ($*$ = 323K, ○ = 298K, □ = 273K). The slopes differ from the true value for k_1 due to the effects of other reactions affecting C_6H_7 with comparable time scales (see section 4.5).

flash photolysis is to determine the C_6H_7 decay time-constants for each absorption experiment, then plot those with respect to the oxygen concentration to obtain a pseudo-first-order approximation of the rate constant, k_1. These decay time-constants are typically calculated by fitting the absorbance signal from its peak using a single-exponential model with an offset

$$y = Ae^{-t/\tau} + B \tag{8}$$

Below a partial pressure of 0.25 atm of O_2, the single-exponential fits to the data were excellent with $R^2 = 0.998$ or above for all parity plots.

Figure 6 shows that the reciprocal of the decay constants for the cyclohexadienyl radical (τ in eq 8) are linearly dependent upon the oxygen concentration. Using linear regression, we derived the pseudo-first-order rate constants for $C_6H_7 + O_2$ at

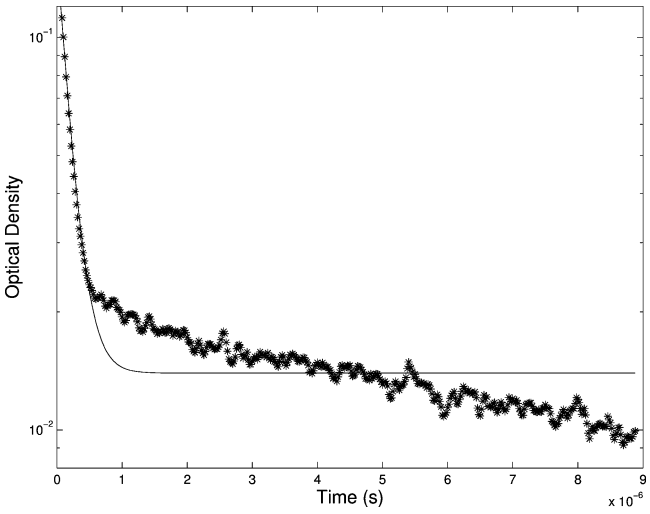

Figure 7. Comparison of cyclohexadienyl decay at 316 nm ($[O_2]$ = 7.5 mM, T = 25 °C) to a single-exponential fit with an offset. Measurements at 316 and 556 nm both show a multiexponential decay, implying that the signal can be attributed to cyclohexadienyl, not an interference.

TABLE 2: Pseudo-First Order Rate Constants for Cyclohexadienyl in Cyclohexane at Several Temperatures

temp [K]	k_1 obtained from eq 8 [M^{-1} s^{-1}]	k_1 obtained from eq 9 [M^{-1} s^{-1}]
273	$9.1 \pm 1.1 \times 10^8$	$1.14 \pm 0.59 \times 10^9$
298	$8.1 \pm 1.8 \times 10^8$	$1.23 \pm 0.31 \times 10^9$
323	$6.3 \pm 0.6 \times 10^8$	$1.22 \pm 0.34 \times 10^9$

various temperatures. These rate constants are listed in Table 2 at various temperatures in cyclohexane solvent.

Although the pseudo-first order rate constants obtained are reasonably close to the diffusion-limit, there are several drawbacks to this approach. First, as the oxygen concentration increases, the time scales for cyclohexadienyl generation and decay become comparable, which causes this procedure to underestimate the true rate constant, k_1. Second, at higher oxygen concentrations, cyclohexadienyl radical decay is not a single exponential, as shown in Figure 7. In section 4.5, several more complex models are used to explain the biexponential decay of Figure 7.

4.5. Models for Cyclohexadienyl Kinetics. Single-exponential models, such as eq 8, make the assumption that there is no generation of the decaying species. Although the generation of C_6H_7 by reaction 6 is on the 100 ns time scale, the decay of C_6H_7 at high $[O_2]$ is almost as fast as its generation. A simple analytical model based on reactions 1 and 6 was constructed to decouple radical decay rates from cyclohexadienyl generation. According to this model

$$[C_6H_7] = \left(\frac{\alpha}{\beta - 1/\tau}\right)e^{-t/\tau} - \left(\frac{\alpha}{\beta - 1/\tau}\right)e^{-\beta t} \qquad (9)$$

where

$$\tau = \frac{1}{k_6[C_6H_8] + k_0}$$

$$\alpha = k_6[(CH_3)_3CO^{\bullet}]_0\,[C_6H_8]_0$$

$$\beta = k_1[O_2]_0 \qquad (10)$$

The constant, k_0, is a fitted parameter to account for all first-order rate processes that are not dependent upon 1,4-cyclohexadiene concentration. Fitting the data measured at 298 K in cyclohexane yielded a $k_1 = 1.23 \pm 0.31 \times 10^9$ M^{-1} s^{-1}, about 50% greater than the value obtained using the conventional approach described in section 4.4.

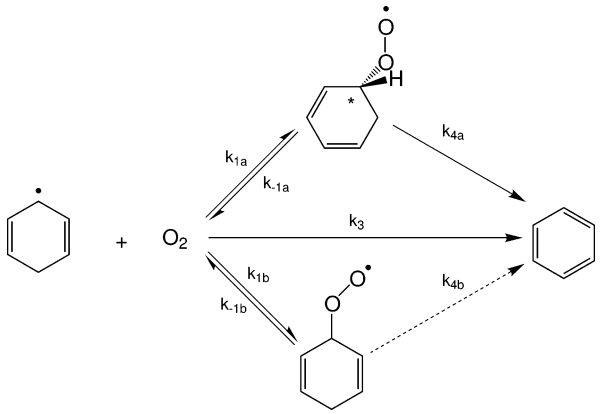

Figure 8. Reaction scheme that is consistent with the observed multiexponential decay of cyclohexadienyl in cyclohexane. The measured data are sufficient to determine $k_1 = k_{1a} + k_{1b}$, but cannot uniquely determine all seven rate constants.

However, the underlying assumption of irreversible forward reactions is not certain and, therefore, requires a more complex reaction network, shown in Figure 8. The inclusion of more reactions (including recombination reactions) into the models improves the agreement with the data, but a purely analytical treatment is no longer feasible. Table 3 lists a series of reactions which were used to create a numerical simulation of cyclohexadienyl kinetics.

Rate constants for the reactions were determined by making several assumptions. First, that the forward rate, k_1, is the diffusion-limited rate constant in cyclohexane, 1.2×10^9 M^{-1} s^{-1}. Second, that reactions 1a and 1b are reversible and that their equilibrium constants can be calculated. Section 5 describes the calculation of these equilibrium constants in more detail. Third, $k_{1a} = 2k_{1b}$ due to the two enantiomers of *o*-C_6H_7OO. Last, a small absorption (200 M^{-1} cm^{-1}) was attributed to cyclohexadienylperoxyl in order to account for the residual baselines observed. All radical recombination rates were assumed to be diffusion-limited, and other rate constants were taken from literature, as cited in Table 3.

Using these values, simulations adequately predicted the overall kinetics of the reactions, as shown in Figures 9 and 10. These parameters were not adjusted to try to improve the fit, as there are not enough data to uniquely determine so many parameters.

5. Results from Theoretical Calculations

5.1. Density Functional Calculations. Ab initio calculations were performed at the B3LYP level to get an estimate of the R−OO bond strength in cyclohexadienylperoxyl radicals, as well as of the free energies of reactions 1a and 1b. Thermal energy contributions and entropies were directly taken from the Gaussian frequency calculations at the B3LYP/6-31G(d) level. Of the six stable minima found on the C_6H_7OO potential energy surface, three structures correspond to *p*-C_6H_7OO and the remaining three to the corresponding *ortho* conformers (see Figure 1 for nomenclature). The conformations which are trans about the C−O bond are 0.9 kcal/mol (*o*-C_6H_7OO) and 1.4 kcal/mol (*p*-C_6H_7OO) more stable than the corresponding gauche

TABLE 3: Important Reactions Used in Simulations of the Present Experiments

#	reaction	k_{298} [M^{-1} s^{-1} or s^{-1}]	refs
6	$(CH_3)_3CO\bullet + 1,4C_6H_8 \rightarrow C_6H_7\bullet + (CH_3)_3COH$	5.3×10^7	43
1b	$C_6H_7\bullet + O_2 \rightarrow$ p- $C_6H_7OO\bullet$	4.0×10^8	6, sec. 3.5
−1b	p- $C_6H_7OO\bullet \rightarrow O_2 + C_6H_7\bullet$	1.9×10^5	sec. 4.3
1a	$C_6H_7\bullet + O_2 \rightarrow$ o- $C_6H_7OO\bullet$	8.0×10^8	6, sec. 3.5
−1a	o- $C_6H_7OO\bullet \rightarrow O_2 + C_6H_7\bullet$	1.9×10^5	sec. 4.3
4a	o- $C_6H_7OO\bullet \rightarrow C_6H_6 + HO_2\bullet$	8×10^5	5
R	$2\ C_6H_7\bullet \rightarrow$ products	1.2×10^9	44

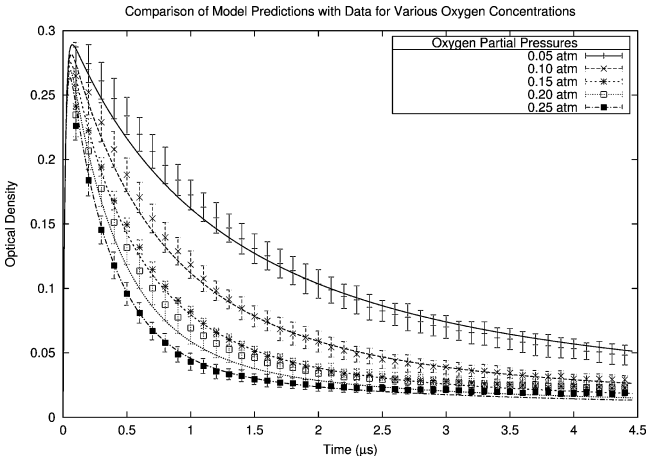

Figure 9. Predictions of a numerical simulation of cyclohexadienyl chemistry at 298K for P_{O_2} ranging from 0.05 to 0.25 atm. Lines represent simulation predictions, while points represent experimental data and their error bars for cyclohexadienyl decay at each oxygen concentration. At low oxygen partial pressures, the equilibrium concentrations of C_6H_7OO and C_6H_7 are comparable, resulting in a large, slowly decaying baseline. Reactions used in the simulation and their rate constants are listed in Table 3.

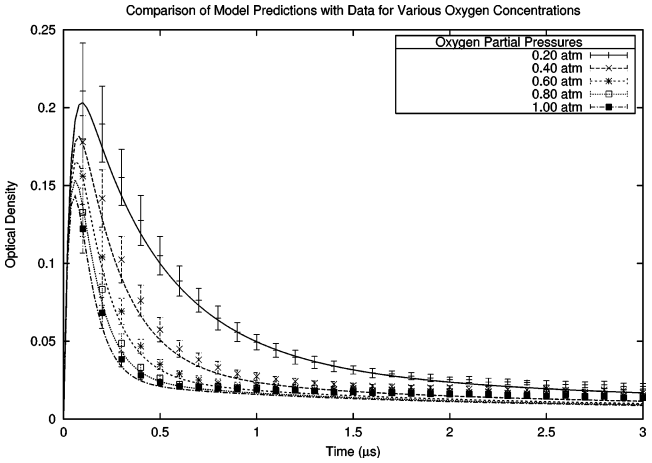

Figure 10. Predictions of a numerical simulation of cyclohexadienyl chemistry at 298 K for P_{O_2} ranging from 0.20 to 1.00 atm. Lines represent simulation predictions, while points represent experimental data and their error bars for cyclohexadienyl decay at each oxygen concentration. At high oxygen concentrations, the equilibrium shifts toward the products of reaction 1, which have a smaller absorption on the order of 200 M^{-1} cm^{-1}. This interference is primarily responsible for the baseline absorbance at higher oxygen concentrations. Reactions used in the simulation and their rate constants are listed in Table 3.

conformations at the B3LYP/6-31G(2df,p) level. The gauche conformers are all comparable in energy to each other. The relative stabilities are insensitive to size of the basis set. The calculated entropy for the reaction using density functional theory (DFT) was determined to be $\Delta S = -35$ cal/mol/K and is similar to other values in the literature.[16]

The enthalpy of the isodesmic reaction 11 was determined using DFT to be $\Delta H° = -8.5$ kcal/mol

$$p\text{-}C_6H_7OO^\bullet + CH_2CHCH_2^\bullet \rightarrow C_6H_7^\bullet + CH_2CHCH_2OO^\bullet \quad (11)$$

Combining this value with the known literature value[40] for the addition of O_2 to allyl ($\Delta H° = -18.5$ kcal/mol), we obtain a bond dissociation energy for $C_6H_7OO \rightarrow C_6H_7 + O_2$ of 10 kcal/mol. Based on other peroxyl radical calculations in the literature, we estimate an uncertainty of 2 kcal/mol for this computed value.

To incorporate solvation effects, we performed polarizable continuum (PCM) calculations with cyclohexane and dichloromethane as solvents. These calculations account for the electrostatic interaction between the dipolar C_6H_7OO and the dielectric medium. This interaction increases the bond strength in cyclohexane solution by 1 kcal/mol.

5.2. Empirical Solvation Corrections. There are additional solvation effects beyond electrostatics (e.g., due to London forces) which are difficult to calculate from first principles. The free energy of solvation of O_2 in many solvents, including cyclohexane, has been measured (in the form of the Henry's Law coefficient, k_{O_2}). Of course, no measurements have been made of the vapor pressure of C_6H_7 and C_6H_7OO radicals. However, their solvation energies and entropies can be estimated from experimental data for other molecules. For example, the enthalpies and entropies of solvation of many stable C_5-C_8 organics in hydrocarbon solvents have been measured using gas−liquid chromatography.[41,42] The difference between the values for nonpolar C_8 and C_6 species falls in a narrow range

$$\Delta\Delta H_{solv} = \Delta H_{solv}^{C_8} - \Delta H_{solv}^{C_6} = -2 \pm 1 \text{ kcal/mol}$$

$$\Delta\Delta S_{solv} = \Delta S_{solv}^{C_8} - \Delta S_{solv}^{C_6} = -2 \pm 1 \text{ cal/mol/K}$$

Excluding electrostatics, the solvation enthalpy of C_6H_7OO and C_6H_7 can be approximated as similar to a C_8 molecule and a C_6 molecule, respectively. Electrostatic effects can then be incorporated using the polarizable continuum model to obtain a solvation enthalpy contribution to reaction 1 of $\Delta\Delta H_{solv} = -3 \pm 1$ kcal/mol. The solvation entropy remains unchanged by PCM and is $\Delta\Delta S_{solv} = -2 \pm 1$ cal/mol/K. Combining these corrections with the gas-phase quantum chemical values, we predict the change in enthalpy for reaction 1 in cyclohexane solution to be -13 ± 3 kcal/mol, consistent with the measurements of -12 ± 1 kcal/mol made by Kranenburg et al.[16] in other organic solvents.

5.3. Summary of Computed Thermochemistry and Equilibria for Reaction 1. To summarize, our best thermodynamic estimates for reaction 1b in gas phase at 298K are as follows:

$$\Delta H^o_{(1b)} = -10 \pm 2 \text{ kcal/mol}$$

$$\Delta S^o_{(1b)} = -35 \pm 1 \text{ cal/mol/K} \quad (12)$$

which corresponds to

$$K_p^o(1\text{ atm, }298\text{K}) = e^{5000\text{ K}/T-18} = 0.5$$

The equilibrium constants for the optical isomers of *o*-C_6H_7-OO are computed to be nearly identical. Because of the error bars in the computed $\Delta H°$ and $\Delta S°$, we can only be certain that $25 \geq K_p^o$ (1 atm, 298 K) ≥ 0.01.

In dilute cyclohexane solution, following the notation of Meyer[41]

$$K_c^o(1\text{ M}) = \frac{[C_6H_7OO^\bullet]}{[C_6H_7^\bullet][O_2]} = \left(\frac{\rho_{C_6H_{12}}K_p}{M_{C_6H_{12}}k_{O_2}}\right)e^{-(\Delta\Delta H_{solv}-T\Delta\Delta S_{solv}/RT)} \quad (13)$$

Evaluating the expression using Suresh's value[24] for k_{O_2} yields the following:

$$K_c^o(1\text{ M, }298\text{ K}) = 46e^{((6500\text{K}/T)-18)} = 2100 \quad (14)$$

The uncertainty in this computed K_c^o is quite large, more than 2 orders of magnitude. However, Kranenburg's experimental data indicate $K_c^o > 100$ in isooctane (otherwise reaction 1a would not proceed forward to any significant extent at the oxygen concentration employed). Our present kinetic data further constrain K_c^o, as discussed below. With the computed K_c^o, if $[O_2] = 476\ \mu$M, the equilibrium concentrations of C_6H_7 and C_6H_7OO are predicted to be equal; in cyclohexane this oxygen concentration will be in equilibrium with an O_2 partial pressure of 0.4 Torr. Most solution phase experiments have been run under much higher O_2 partial pressures of 76−760 Torr, where the equilibrium is predicted to strongly favor C_6H_7OO over C_6H_7, consistent with the observed rapid disappearance of C_6H_7.

6. Discussion

6.1. Comparison with Previous Liquid-Phase Experiments. Experimental data obtained in these experiments are comparable to other liquid-phase studies, which all conclude that reaction 1 is diffusion-limited in their respective solvents. The current experiments determine the rate constant for reaction 1 in cyclohexane (see Table 2).

In comparison to the values in Table 2, Maillard's rate constant[6] in benzene at 298K was determined to be 1.67×10^9 M^{-1} s^{-1}. Multiplying Maillard's rate constant by the ratio of benzene/cyclohexane viscosities, gives an expected rate constant of 1.1×10^9 M^{-1} s^{-1}, within the expected error bars of the corrected values in Table 2. Using the Stokes−Einstein relation between diffusivity and viscosity, the diffusion-limited rate constant in cyclohexane was calculated to be 1.5×10^9 M^{-1} s^{-1} at 298 K, within 50% of the measured rate constants.

Hendry[17] proposed that the major products of the fast reaction of C_6H_7 and O_2 in the liquid-phase are benzene and HO_2. However, Pan[5] and Maillard[6] proposed that C_6H_7OO is the primary product of the reaction. Pan also observed that, in aqueous solution, HO_2 generation was significantly slower than the cyclohexadienyl decay, implying an intermediate step. However, the most convincing evidence that C_6H_7OO is the main product in the liquid-phase comes from thermodynamic data determined by Kranenburg et al. using photoacoustic calorimetry. Kranenburg determined in organic solvents, at microsecond time scales, that the decay of cyclohexadienyl radicals generated 12 kcal/mol of energy. This is consistent with the calculated enthalpy of reaction 1, but much less than the 23 kcal/mol expected if the dominant products were HO_2 and C_6H_6. At this time-scale, reaction 1 must dominate other pathways with greater heats of reaction.

6.2. Deviation from Single-Exponential Behavior and Equilibrium. Single exponential decay models do not adequately fit the data as shown in Figure 7. Both the 316 and 556 nm bands exhibit the same multiexponential decay with time, indicating that the signal must be attributable to the cyclohexadienyl radical itself or to another molecule in equilibrium with cyclohexadienyl on the sub-microsecond time scale, as opposed to interference by other molecules.

Based on these results and our thermochemistry calculations, we propose that reactions 1 are in equilibrium under our reaction conditions

$$C_6H_7^\bullet + O_2 \rightleftharpoons o\text{-}C_6H_7OO^\bullet \quad (1a)$$

$$C_6H_7^\bullet + O_2 \rightleftharpoons p\text{-}C_6H_7OO^\bullet \quad (1b)$$

A similar equilibrium has been proposed for hydroxycyclohexadienyl by von Sonntag.[45] A possible explanation for the oxygen-dependent multiexponential decay could be the C_6H_7 radical coming into equilibrium with the corresponding peroxyl radicals, followed by a slower decay of the equilibrated radicals. The experimental data in cyclohexane suggests that reaction 1 becomes equilibrated within 2−3 μs for $[O_2] > 2.5$ mM.

6.3. Experimental Bounds on Equilibrium 1. Our best information on the equilibrium constant for reaction 1 in the gas-phase comes from the calculations discussed in section 6.3. However, experiments also allow bounds on K_c^o to be determined in solution. The experiments of Kranenburg et al.[16] prove that, at high oxygen concentrations, most of the C_6H_7 is converted into C_6H_7OO on a sub-microsecond time scale, bounding $K_c^o > 100$ in isooctane and ethyl acetate. The present experiments provide tighter bounds on K_c^o in solution. The observation that C_6H_7 is quantitatively converted by reaction with O_2 even at sub-atmospheric concentrations of O_2, indicates that $K_c^o > 1 \times 10^3$.

As discussed above, we attribute the fast component of the biexponential decay to equilibration of reaction 1. With this interpretation of the data, the ratio of the amplitudes of the slow to the fast components of the multiexponential in principle provides a direct measure of $K_c^o/[O_2]$. However, accurate measurement of this ratio is only feasible over a limited range, and there are several interferences and secondary reactions which need to be modeled in order to extract a value for K_c^o. From these bounds and the simulations at 298 K, we derive

$$2 \times 10^4 > K_c^o\text{ (1 M, 298 K)} > 1 \times 10^3 \quad (15)$$

The temperature dependence of K_c^o derived by the fitting procedure over the range 0−50 °C is consistent with the measured[16] and calculated values of $\Delta H = 12-13$ kcal/mol, but the kinetic data are not sufficient to determine ΔH more precisely. In other words, the data indicate that $k_{-1b} \approx 2 \times 10^5$ s^{-1} at 298 K, with an $E_a \approx 12$ kcal/mol. The corresponding $A \sim 10^{14}$ s^{-1} is in the range expected for a barrierless dissociation. The large A factor for the reverse reaction and the observation that reaction 1 is diffusion-controlled even in low viscosity, weakly interacting solvents at 273 K strongly suggest that reaction 1 has no significant barrier in nonpolar solvents. In the gas phase, however, several published quantum chemical calculations[13,14] and a recent study on hydroxycyclohexadienyl[46] report barriers to this reaction.

TABLE 4: Comparison of Inferred Reaction 1 and Reaction 2 Equilibrium Constants

equilibrium constants at 25 °C	reaction 1	reaction 2
K_p^o (1 atm)	0.5	0.14[a]
K_c^o (1 M)	2.1×10^3 [b]	2.5×10^3 [c]

[a] Bohn in 1999, ref 8. [b] Cyclohexane Solvent, present work. [c] Pan, 1988 in Water, ref 5.

The calculations in section 5.3 predict that 2 atm of O_2 are required to convert half of the gas-phase C_6H_7 to C_6H_7OO at equilibrium, while a partial pressure of only 0.05 atm would suffice to achieve that condition in cyclohexane solution. This predicted 2 orders of magnitude variation between the behavior in solution and in the gas phase is consistent with all experimental data on reaction 1 and similar to that observed experimentally for reaction 2.[8,12] It is interesting to directly compare the literature equilibrium constants for reaction 2 with our calculated values for reaction 1, as shown in Table 4.

6.4. Subsequent Reactions Responsible for the Overall Decay of C_6H_7 at Equilibrium Conditions. At least two possible mechanisms exist that can explain the decay of C_6H_7 after reactions 1 equilibrate. Pan et al. have proposed that the product of reaction 1a, *o*-C_6H_7OO, decomposes irreversibly through reaction 4a. Reaction 4b is expected to be much slower and can be neglected in this model. Berho and Lesclaux,[3] and more recently Estupiñán,[4] proposed reaction 3, the direct abstraction of a hydrogen from cyclohexadienyl, as the dominant loss channel in the gas phase. Both these potential pathways are shown in Figure 8.

6.4.1. Analysis of the Overall Decay in the Gas Phase. Using the calculated equilibria determined in section 5.3 for reactions 1a and 1b, reported gas-phase experiments[3,4] operate in a regime where the equilibria strongly favor C_6H_7 over C_6H_7OO. Thus, only a negligible amount of C_6H_7 is consumed before equilibrium is reached. The observed experimental decay of C_6H_7 to C_6H_6 and HO_2 ($k_{exp} = 8.4 \times 10^7 \exp(-0.6\ \text{kcal/RT})\ M^{-1}\ s^{-1}$) must primarily be due to either reaction 3 and/or reaction 4a.

Using the quasi-steady-state approximation on the peroxyl radical intermediates, allows the determination of a rate-law for the gas phase, as shown in eq 16:

$$\frac{d[C_6H_7]}{dt} = \left(\frac{k_{-1a}k_{1a}}{k_{-1a}+k_{4a}} - (k_{1a}+k_3)\right)[C_6H_7][O_2] \quad (16)$$

Several direct conclusions can be made using eq 16. First, the decay in the gas-phase cannot be due to k_{1a} alone. In order for this to be true, $k_{4a} \gg k_{-1a}$, such that $k_{exp} \sim k_{1a}$. However, for k_{1a} to be the primary loss channel, the reaction rate would have to decrease by 2 orders of magnitude from the liquid phase to the gas phase. The observed small activation energy of 0.6 kcal/mol is inconsistent with such a large change in reaction rate.

Second, if, on the other hand, $k_{-1a} \gg k_{4a}$, then the direct abstraction of hydrogen (reaction 3) is the primary pathway in the gas phase, as stated by Estupiñán et al.[4] The low value of the rate constant coupled with the small activation barrier is unusual for H abstraction, but this reaction is atypical in many respects.

However, a final possibility exists: Pan argues that peroxyl rearrangement to form benzene and HO_2 (1) dominates the direct abstraction pathway (3) but not the equilibrium back reaction (-1). The observed decay could then be explained by equilibrium 1 in combination with the decomposition of *o*-C_6H_7OO

$$\frac{d[C_6H_7]}{dt} = -\left(\frac{k_{1a}k_{4a}}{k_{-1a}+k_{4a}}\right)[C_6H_7][O_2] \quad (17)$$

The weak temperature dependence would in this case be due to the overall decay being a combination of the exothermic equilibrium 1 and the endothermic reaction 4a. Of course, it is also possible that both reactions 4a and 3 contribute comparably to the overall decay and that this combination would also exhibit little temperature dependence. The available experimental data are currently not sufficient to determine whether reaction 3 or reaction 4a is dominant in the gas phase. Since the dominant reaction pathway is in doubt, we recommend the use of eq 16, which allows for both channels in interpreting experimental data.

6.4.2. Analysis of the Overall Decay in the Liquid Phase. Unfortunately, on the short time scale of the liquid-phase experiments, the steady-state approximation cannot be applied to the peroxyl intermediates, significantly complicating the interpretation of the data. However, a perturbation analysis of the cyclohexadienyl kinetic model in Figure 8 does provide analytical approximations for the eigenvalues of the system. The following parameters correspond to the calculated zeroth- and first-order terms of the eigenvalues, where the small parameters were defined as k_3/k_{-1b} and k_{4a}/k_{-1b}

$$\lambda_1 = -k_{-1a} - (k_{1a}+k_{1b})[O_2] - \frac{k_3(K_{1a}+K_{1b})[O_2]^2}{(1+(K_{1a}+K_{1b})[O_2])} - \frac{2k_{4a}}{3(1+(K_{1a}+K_{1b})[O_2])} \quad (18)$$

$$\sim -(k_{1a}+k_{1b}+k_3)[O_2] \quad (19)$$

$$\lambda_2 = -\left(k_{-1a} + \frac{k_{4a}K_{1b}}{K_{1a}+K_{1b}}\right) \quad (20)$$

$$\sim -\left(k_{-1a} + \frac{k_{4a}}{3}\right) \quad (21)$$

$$\lambda_3 = -\left(\frac{(k_3 + k_{4a}K_{1a})[O_2]}{1+(K_{1a}+K_{1b})[O_2]}\right) \quad (22)$$

$$\sim -\frac{2k_{4a}}{3} \quad (23)$$

The approximations are valid when $k_{1b}[O_2] \gg 1$, and assume $k_{1a} \approx 2k_{1b}$. The fast component of C_6H_7 decay observed in solution is dominated by the title reaction. However, several other effects compete in addition to the effects of convolution with the time constant of the decay of *tert*-butoxyl in the formation of C_6H_7 discussed in section 4.4.

Once reactions 1a and 1b reach equilibrium, the observed cyclohexadienyl decay occurs with time constants corresponding to $1/\lambda_2$ and $1/\lambda_3$, which both are functions of k_{4a}. Note that λ_3 is similar, but not identical to eq 16; both agree that pathway 3 is favored if $k_{1b}[O_2]$ is small, whereas pathway 1 is favored if $k_{1b}[O_2]$ is large. The temperature dependence in the slow component of cyclohexadienyl decay, shown in Figure 5, thus depends mainly on the interplay between the back reaction, -1a, and the reactions which lead to HO_2 and C_6H_6, 3 and 4a. The large increase in the slow component decay observed between 298K and 323K would be consistent with an emergence of $\lambda_2 \sim -k_{-1a}$, since reaction -1 is expected to have a high activation

barrier. The difficulties with determining the relationship between the measured time constants of the C_6H_7 decay in the presence of oxygen, and the underlying elementary steps, suggests that theoretical estimates of the rate constants, not just the thermochemistry, are necessary to understand this system in detail.

6.4.3. Estimates for Rate Constants. Reactions 1 and 3. All solution-phase experiments agree that the reaction of the cyclohexadienyl radical with oxygen is diffusion-limited. The experiments performed in this work determine this rate constant to be $\approx 1.2 \times 10^9$ M^{-1} s^{-1}. Due to the statistical factor associated with the *ortho* and *para* forms, we expect $k_{1a} \approx 2k_{1b}$, making $k_{1a} \approx 8 \times 10^8$ M^{-1} s^{-1} and $k_{1b} \approx 4 \times 10^8$ M^{-1} s^{-1}. Using the computed K_c, we infer k_{-1a} (for each enantiomer) and k_{-1b} to range from 0.4 to 8×10^5 s^{-1} at 298 K. The rate constant k_3 must be less than 3×10^8 M^{-1} s^{-1} in solution to be consistent with Kranenburg's calorimetry data and our calculated thermochemistry, taking error bars into account. The fact that reactions 1a and 1b appear to be diffusion-controlled indicates that the intrinsic chemistry rates are faster than the diffusion rate. In the gas phase, A factors for $R + O_2$ reactions are normally in the range of 10^9 to 10^{10} M^{-1} s^{-1}; if k_1 has a similar A factor, yet $k_{intrinsic} > k_{diff} \approx 1 \times 10^9$ M^{-1} s^{-1} at $T = 0$ °C we can infer that $E_a < 1.3$ kcal mol^{-1} (in solution). There is likely some solvent effect on the E_a for reaction 1 similar to that on the product C_6H_7OO, which could increase the barrier in the gas phase. However, the fact that the analogous allyl radical reaction with O_2 in the gas phase at room temperature is known to be quite fast (3.6×10^8 M^{-1} s^{-1})[47] suggests the true gas-phase E_a for reaction 1 is 2 kcal/mol or less. Some quantum calculations reported in the literature show high barriers to reactions 1 and 2. However, long-distance floppy transition states that involve considerable changes in electronic structure are extremely difficult to compute accurately. The more plausible hypothesis can be based on experimental analogy with allyl radical and the fact that this reaction runs at the diffusion-limited rate even in weakly interacting nonpolar solvents.

Little is known theoretically regarding reaction 3, which is much more exothermic than typical H-abstractions by O_2. The floppy bi-radical transition state is expected to be extremely difficult to calculate accurately with available quantum chemistry techniques. Normal *A* factors for H-abstractions and radical−radical disproportionations are typically $\sim 10^9$ M^{-1} s^{-1}. If reaction 3 has an *A* factor in this range, $k_3 < 3 \times 10^7$ M^{-1} s^{-1} in the gas phase would imply $E_a > 2.3$ kcal/mol in the gas phase, comparable with barriers seen in comparably exothermic H-abstractions by OH. Less is known about the barrier to reaction 3 in solution phase; if we again assume $A_3 \sim 10^9$ M^{-1} s^{-1}, we infer that $E_a > 0.6$ kcal/mol in order to be consistent with the experimental upper bound on k_3.

Reactions 4a and 4b. Almost nothing is known for certain about reactions 4. The A factor for reaction 4a is probably similar to the 5×10^{11} s^{-1} A factor for the analogous reaction

$$C_2H_5OO \rightleftharpoons C_2H_4 + HO_2 \qquad (24)$$

which has been thoroughly studied experimentally[18] and theoretically.[1,48] However, the barrier height is certainly very different, since the thermochemistry of reaction 24 is dramatically different than that for reaction 4a. An upper bound on k_{4a} can be determined, however, using eq 17. This bounds k_{4a} and $k_{4b} < 1 \times 10^6$ s^{-1} in the gas phase at $T = 298$ K and they must be even less if there is competition with k_3.

7. Conclusions

Several conclusions can be drawn from this work:

1. The weak 556 nm band has identical time-dependence as the stronger 316 nm band, which suggests that both bands arise from the cyclohexadienyl radical.

2. In most solvents, k_1 is close to the diffusion limit, implying that no significant barrier to reaction exists. This is contrary to several quantum chemical calculations in the literature, which report significant barriers to resonantly stabilized $R + O_2$ reactions. However, it is consistent with other experimental data on $R + O_2$ reactions, particularly those reactions in solution.

3. In contrast to previous reports, cyclohexadienyl radical decay is not a single-exponential decay. The multiexponential decay is due to equilibration of reaction 1, followed by slow decay of the equilibrated system.

4. The equilibrium constant of reaction 1 has been computed. Under low oxygen concentrations, the computed value favors the reactants in most gas-phase experiments. In contrast, at the higher oxygen concentrations of liquid-phase experiments, equilibrium favors the products, in part due to solvation effects.

5. Gas phase experiments measure the rate of a process other than reaction 1. We propose these experiments actually measure the combination of rate constants shown in eq 16. If reactions 1 or 4a are negligible in gas phase, then reaction 3, as proposed by Estupiñán,[4] is the dominant pathway. Available data are insufficient to determine the primary peroxyl decay channel.

The title reaction provides a dramatic example of the importance of nonspecific solvation effects, even for free radical reactions in weakly interacting nonpolar solvents.

Acknowledgment. We are very grateful to ExxonMobil Research and Engineering Co. for loaning us some of the equipment used to make these measurements. Additional equipment loans and support from the Harrison Spectroscopy Laboratory are also gratefully acknowledged. We are grateful to David M. Matheu for performing the pressure-dependence calculations on our behalf, and to Joseph W. Bozzelli, Anthony M. Dean, and John R. Barker for providing software employed in the course of this work. G.E. is grateful to the University of Aachen, Germany, which supported his work at MIT. J.T. is grateful to the National Science Foundation for providing support for this work through a pre-doctoral fellowship. This work was supported by the U.S. Department of Energy's Basic Energy Sciences program, and by grants from the National Science Foundation and the Edgerly Science Partnership Fund.

References and Notes

(1) Rienstra-Kiracofe, J. C.; Allen, W. D.; Schaefer, H. F. *J. Phys. Chem. A* **2000**, *104*, 9823−9840.

(2) Desain, J. D.; Taatjes, C. A.; Miller, J. A.; Klippenstein, S. J.; Hahn, D. K. *Faraday Discuss.* **2001**, *119*, 101−120.

(3) Berho, F.; Lesclaux, R. *Phys. Chem. Chem. Phys.* **2001**, *3*, 970−979.

(4) Estupiñán, E.; Villenave, E.; Raoult, S.; Rayez, J. C.; Rayez, M. T.; Lesclaux, R. *Phys. Chem. Chem. Phys.* **2003**, *5*, 4840−4845.

(5) Pan, X.-M.; Schuchmann, M. N.; von Sonntag, C. *J. Chem. Soc., Perkins Trans.* **1993**, *2*, 1021−1028.

(6) Maillard, B.; Ingold, K. U.; Scaiano, J. C. *J. Am. Chem. Soc.* **1983**, *105*, 5095−5099.

(7) Bjergbakke, E.; Sillesen, A.; Pagsberg, P. *J. Phys. Chem.* **1996**, *100*, 5729−5736.

(8) Bohn, B.; Zetzsch, C. *Phys. Chem. Chem. Phys.* **1999**, *1*, 5097−5107.

(9) Berndt, T.; Böge, O. *Phys. Chem. Chem. Phys.* **2001**, *3*, 4946−4956.

(10) Johnson, D.; Raoult, S.; Rayez, M.-T.; Rayez, J.-C.; Lesclaux, R. *Phys. Chem. Chem. Phys.* **2002**, *4*, 4678−4686.

(11) Pan, X.; Bastian, E.; von Sonntag, C. *Z. Naturforsch., B−J. Chem. Sci.* **1988**, *43*, 1201−1205.

(12) Fang, X.; Pan, X.; Rahmann, A.; Schuchmann, H.-P.; von Sonntag, C. *J. Eur. Chem.* **1995**, *1*, 423−429.

(13) Andino, J.; Smith, J.; Flagan, R.; Goddard, W.; Seinfeld, J. *J. Phys. Chem.* **1996**, *100*, 10967−10980.
(14) Ghigo, G.; Tonachini, G. *J. Am. Chem. Soc.* **1998**, *120*, 6753−6757.
(15) Zils, R.; Inomata, S.; Imamura, T.; Miyoshi, A.; Washida, N. *J. Phys. Chem. A* **2001**, *105*, 1277−1282.
(16) Kranenburg, M.; Ciriano, M. V.; Cherkasov, A.; Mulder, P. *J. Phys. Chem. A* **2000**, *104*, 915−921.
(17) Hendry, D.; Schuetzle, D. *J. Am. Chem. Soc.* **1975**, *97*, 7123−7127.
(18) Kaiser, E. W. *J. Phys. Chem. A* **2002**, *106*, 1256−1265.
(19) Taatjes, C.; Klippenstein, S. *J. Phys. Chem. A* **2001**, *105*, 8567−8578.
(20) Lay, T.; Bozzelli, J.; Seinfeld, J. *J. Phys. Chem.* **1996**, *100*, 6543−6554.
(21) Raoult, S.; Rayez, M.-T.; Rayez, J.-C.; Lesclaux, R. *Phys. Chem. Chem. Phys.* **2004**, *6*, 2245−2253.
(22) Benson, S. W. *J. Am. Chem. Soc.* **1965**, *87*, 972−79.
(23) Wilhelm, E.; Battino, R. *J. Chem. Thermodyn.* **1973**, *5*, 117−120.
(24) Suresh, A. K.; Sridhar, T.; Potter, O. E. *AIChE J.* **1988**, *34*, 55−68.
(25) King, P. "Pro-K: global analysis and simulation software for Acorn Risc based computer", Applied Photophysics, Leatherhead, U.K., 1996.
(26) Frisch, M. J.; Trucks, G. W.; Schlegel, H. B.; Scuseria, G. E.; Robb, M. A.; Cheeseman, J. R.; Zakrzewski, V. G.; Montgomery, J. A., Jr.; Stratmann, R. E.; Burant, J. C.; Dapprich, S.; Millam, J. M.; Daniels, A. D.; Kudin, K. N.; Strain, M. C.; Farkas, O.; Tomasi, J.; Barone, V.; Cossi, M.; Cammi, R.; Mennucci, B.; Pomelli, C.; Adamo, C.; Clifford, S.; Ochterski, J.; Petersson, G. A.; Ayala, P. Y.; Cui, Q.; Morokuma, K.; Malick, D. K.; Rabuck, A. D.; Raghavachari, K.; Foresman, J. B.; Cioslowski, J.; Ortiz, J. V.; Stefanov, B. B.; Liu, G.; Liashenko, A.; Piskorz, P.; Komaromi, I.; Gomperts, R.; Martin, R. L.; Fox, D. J.; Keith, T.; Al-Laham, M. A.; Peng, C. Y.; Nanayakkara, A.; Gonzalez, C.; Challacombe, M.; Gill, P. M. W.; Johnson, B. G.; Chen, W.; Wong, M. W.; Andres, J. L.; Head-Gordon, M.; Replogle, E. S.; Pople, J. A. *Gaussian 98*, revision A.9; Gaussian, Inc.: Pittsburgh, PA, 1998.
(27) Foresman, J. B.; Keith, T. A.; Wiberg, K. B.; Snoonian, J.; Frisch, M. J. *J. Phys. Chem.* **1996**, *100*, 16098−16104.
(28) Wijaya, C. D.; Sumathi, R.; Green, W. H. *J. Phys. Chem. A* **2003**, *107*, 4908−4920.
(29) Pilling, M.; Seakins, P. *Reaction Kinetics*; Oxford University Press: Oxford, 1995.
(30) Slagle, I. R.; Ratajczak, E.; Heaven, M. C.; Gutman, D.; Wagner, A. F. *J. Am. Chem. Soc.* **1985**, *107*, 1838−1845.
(31) Ritter, E. R.; Bozelli, J. W. *Int. J. Chem. Kinet.* **1991**, *23*, 767−778.
(32) Barker, J. R. "MultiWell-1.3.1 software", http://aoss.engin.umich.edu/multiwell/: Ann Arbor, MI, 2003.
(33) Barker, J. R. *Int. J. Chem. Kinet.* **2001**, *33*, 232−45.
(34) Stein, S.; Rabinovitch, B. *J. Chem. Phys.* **1973**, *58*, 2438−2445.
(35) Bell, E. R.; Rust, F. F.; Vaughan, W. E. *J. Am. Chem. Soc.* **1950**, *72*, 337−38.
(36) Sauer, Jr, M. C.; Ward, B. *J. Phys. Chem.* **1967**, *71*, 3971−3983.
(37) Simic, M.; Hayon, E. *J. Phys. Chem. A* **1971**, *75*, 1677−1680.
(38) Tsentalovich, Y. P.; Kulik, L. V.; Gritsan, N. P.; Yurkovskaya, A. V. *J. Phys. Chem. A* **1998**, *102*, 7975−7980.
(39) Jordan, J. E.; Pratt, D. W.; Wood, D. E. *J. Am. Chem. Soc.* **1974**, *96*, 5588−5590.
(40) Sheng, C. Y.; Bozelli, J. W.; Dean, A. M.; Chang, A. Y. *J. Phys. Chem. A* **2002**, *106*, 7276−7293.
(41) Meyer, E.; Stec, K.; Hotz, R. *J. Phys. Chem.* **1973**, *77*, 2140−2145.
(42) Meyer, E. *J. Chem. Educat.* **1973**, *50*, 191−194.
(43) Effio, A.; Griller, D.; Ingold, K.; Scaiano, J.; Sheng, S. *J. Am. Chem. Soc.* **1980**, *102*, 6063−6068.
(44) Arends, I. W. C. E.; Mulder, P.; Clark, K. B.; Wayner, D. D. M. *J. Phys. Chem.* **1995**, *99*, 8182−8189.
(45) von Sonntag, C.; Schuchmann, H.-P. *Angew. Chem.−Int. Ed.* **1991**, *30*, 1229−1253.
(46) Grebenkin, S. Y.; Krasnaperov, L. N. *J. Phys. Chem. A* **2004**, *108*, 1953−1963.
(47) Jenkin, M. E.; Murrells, T. P.; Shalliker, S. J.; Hayman, G. D. *J. Chem. Soc., Faraday Trans.* **1993**, *89*, 433−446.
(48) Miller, J.; Klippenstein, S.; Robertson, S. *Proc. Combust. Inst.* **2000**, *28*, 1479−1486.